N-photon bundle statistics on different solid-state platforms

N-photon bundle statistics on different solid-state platforms

M. Cosacchi,[1] A. Mielnik-Pyszczorski,[1,2] T. Seidelmann,[1] M. Cygorek,[3] A. Vagov,[1] D. E. Reiter,[4] and V. M. Axt[1]
[1]*Theoretische Physik III, Universität Bayreuth, 95440 Bayreuth, Germany*
[2]*Department of Theoretical Physics, Wrocław University of Science and Technology, 50-370 Wrocław, Poland*
[3]*Heriot-Watt University, Edinburgh EH14 4AS, United Kingdom*
[4]*Institut für Festkörpertheorie, Universität Münster, 48149 Münster, Germany*

(Received 21 February 2022; revised 1 July 2022; accepted 26 August 2022; published 14 September 2022)

The term N-photon bundles has been coined for a specific type of photon emission, where light quanta are released from a cavity only in groups of N particles. This emission leaves a characteristic number distribution of the cavity photons that may be taken as one of their fingerprints. We study this characteristic N-photon bundle statistics considering two solid-state cavity quantum electrodynamics (cQED) systems. As one example, we consider a semiconductor quantum-dot–microcavity system coupled to longitudinal acoustic phonons. There, we find the environmental influence to be detrimental to the bundle statistics. The other example is a superconducting qubit inside a microwave resonator. In these systems, pure dephasing is not important and an experimentally feasible parameter regime is found, where the bundle statistics prevails.

DOI: 10.1103/PhysRevB.106.115304

I. INTRODUCTION

Many innovative applications of the quantum realm rely on the on-demand preparation of specific, highly nonclassical target states. Cavity quantum electrodynamics (cQED) is a well established tool for this purpose. On numerous different platforms, e.g., atoms in resonators [1–3], superconducting qubits in microwave resonators [4,5], or semiconductor quantum dots in microcavities [6–26], preparation of single photons, entangled photon pairs, Fock states, and Schrödinger or Voodoo cat states has been proposed or achieved. Recently, a new class of emitters has been proposed [27,28], where the photon emission takes place only in groups of an integer number N. The term N-photon bundle has been coined to describe these multiphoton structures. There are numerous ways to characterize these structures, e.g., in terms of their emission properties [29,30] or their internal correlations between the constituent photons [31], which can be interpreted as a consequence of their specific temporal spacing, see sketch in Fig. 1. In contrast to the ordinary Fock state $|N\rangle$, a bundle is emitted as a cascade over successive Fock states $|n\rangle$, where $0 \leqslant n \leqslant N$, after the preparation of the state $|N\rangle$. The cascade is a direct result of the outcoupling via resonator losses. In a resonator with loss rate κ, the Fock state $|n\rangle$ effectively decays with the rate $n\kappa$, explaining the temporal spacing between the photons constituting the bundle. A feature that has been established in Ref. [27] as a major fingerprint of an N-photon bundle, resulting from its cascaded generation, is its characteristic stationary photon statistics:

$$P_N(n) = \begin{cases} 1 - \frac{\langle n\rangle}{N}\sum_{j=1}^{N}\frac{1}{j} & n = 0 \\ \frac{\langle n\rangle}{N}\frac{1}{n} & 1 \leqslant n \leqslant N \\ 0 & n > N \end{cases} \tag{1}$$

with $\langle n\rangle$ being the average photon number in the resonator. Note that the stationary distribution of photon number states is directly accessible to experiments [32–34], and thus the statistics given by Eq. (1) is a measurable quantity.

The N-photon bundle is highly nonclassical and exhibits two attractive properties: (i) a sharp cutoff for photon number occupation probabilities $P_N(n)$ with $n > N$ and (ii) it contains a relatively high stationary N-photon component. The cutoff is useful for applications, e.g., in quantum cryptography [35]. A simultaneous creation of N photons is advantageous for medical applications due to a greater penetration depth and better resolution [27,36–40]. On timescales longer than the size of the bundle, Planck's constant is effectively renormalized in the relationship between frequency and energy, $E = N\hbar\omega$. Since in a stationary state an N-photon component is always redistributed to states with lower $n < N$ due to cavity losses, the characteristic bundle statistics according to Eq. (1) reflects both important properties.

Cavity losses are both unavoidable and necessary for actual quantum technological applications, because, typically, the photon state created inside the cavity has to be delivered to a recipient outside the cavity structure. Although the target N-photon component in the stationary bundle state is lower than subsequent n-photon components [cf. Eq. (1) for $n < N$], it still realizes the highest possible relative N-photon component that can be achieved in a stationary situation with loss processes. In this sense, the N-photon bundle is probably the best compromise between creating a pure N-photon Fock state $|N\rangle$ only inside the cavity and delivering a high N-photon component in a stationary fashion.

From a detection point of view this means the following: When a Poissonian source emits photons, their arrival times at the detector are distributed randomly; in the case of an N-photon bundle emission, the bundles arrive randomly, but the photons contained in each bundle obey the temporal order as sketched in Fig. 1. Therefore there is a Poissonian distribution over bundles. In this sense, N-photon bundles can be

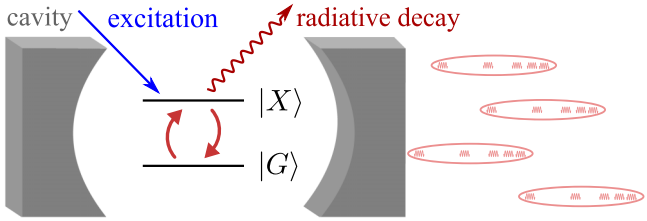

FIG. 1. Sketch of a two-level system (2LS) embedded in a cavity resulting in the coupling to one cavity mode. The 2LS is driven by a continuous external excitation. It can decay radiatively, while the cavity is lossy. For particular sets of parameters, N-photon bundles leave the cavity. They are characterized by the specific temporal spacing between the constituent photons and their specific photon number statistics. Exemplary, four five-photon bundles are depicted.

considered as an alternative to Fock states as building blocks for more complex quantum states of light. In addition to optical applications, even bundle generation using phonons instead of photons has been proposed [41].

In this work, we consider the bundle statistics in Eq. (1) as one of the possible ways to characterize a bundle and study this fingerprint in two different solid-state platforms: (i) semiconductor quantum dots (QDs) in microcavities and (ii) superconducting qubits in microwave resonators.

In QDs, the coupling to longitudinal acoustic phonons is known as the main source of decoherence. Furthermore, phonon emission and absorption can assist off-resonant single-photon processes and, thus, influence the competition between these processes and direct higher-order multi-photon processes [42]. Because the N-photon bundle is associated with an N-photon resonance, phonons can impact the bundle generation. We therefore analyze a QD–cavity system coupled to a phonon environment modeled in a microscopic picture. This full many-body problem is solved in a numerically exact way by employing a path-integral formalism. We compare these results with those found in a model accounting for phonons only via a phenomenological pure dephasing rate. For realistic parameters that are currently achievable, we find that the phonon influence leads to photon number distributions that deviate significantly from the bundle statistics in Eq. (1).

In superconducting qubit–microwave resonator systems, pure dephasing is negligible. For these systems, we propose a set of parameters experimentally well within reach, where the bundle statistics with $N = 2$ is preserved. We show that for this purpose a resonator with a mediocre Q factor is optimal.

II. MODEL AND METHODS

A. cQED model

Both example systems can be described by a strongly driven Jaynes–Cummings model with the Hamiltonian in a frame corotating with the frequency of the external excitation ω_{L} in the usual dipole and rotating-wave approximations

$$\begin{aligned} H_{\mathrm{Sys}} = & -\hbar\Delta\omega_{\mathrm{LX}}|X\rangle\langle X| + \hbar\Delta\omega_{\mathrm{CL}}a^{\dagger}a \\ & + \hbar g(|X\rangle\langle G|a + |G\rangle\langle X|a^{\dagger}) \\ & + \hbar f(|X\rangle\langle G| + |G\rangle\langle X|). \end{aligned} \tag{2}$$

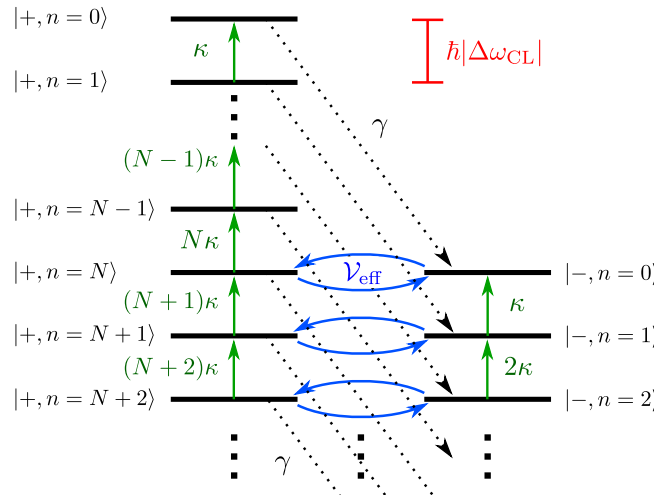

FIG. 2. Schematic sketch of the N-bundle mechanism. Black lines indicate the energetic position of systems states $|\pm,n\rangle$ where the driven 2LS is in the upper (lower) laser-dressed state $|+\rangle \approx |X\rangle$ ($|-\rangle \approx |G\rangle$) and $n \in \mathbb{N}_0$ photons are inside the resonator. Note that in the rotating frame the contribution of a resonator photon $\hbar\Delta\omega_{\mathrm{CL}}$ to the total energy is negative in the regime where bundles are found (cf. Fig 3). The states $|-,0\rangle$ and $|+,N\rangle$ are in resonance and the resonator introduces an effective coupling $\mathcal{V}_{\mathrm{eff}}$ between them (blue arrows). Green (dashed black) arrows indicate the action of the resonator loss (radiative decay) with rate $n\kappa$ (γ) on a system state $|\pm,n\rangle$.

The two-level system (2LS) has an excited state $|X\rangle$ at energy $\hbar\omega_{\mathrm{X}}$ and a ground state $|G\rangle$ at energy zero. a ($a^{\dagger}$) is the annihilation (creation) operator of a photon in the single resonator mode at energy $\hbar\omega_{\mathrm{C}}$ coupled to the 2LS by g. The detuning between the external excitation with strength f and the upper state $|X\rangle$ is denoted by $\Delta\omega_{\mathrm{LX}} = \omega_{\mathrm{L}} - \omega_{\mathrm{X}}$ and the detuning between resonator and external excitation $\Delta\omega_{\mathrm{CL}} = \omega_{\mathrm{C}} - \omega_{\mathrm{L}}$ is defined analogously. The detuning between resonator and the upper state $|X\rangle$, $\Delta\omega_{\mathrm{CX}} = \omega_{\mathrm{C}} - \omega_{\mathrm{X}}$, is fixed by the growth process of the structure. Hence, we keep it constant in our analysis.

When the 2LS is strongly driven ($f \gg g$) and it is in the dispersive regime ($\Delta\omega_{\mathrm{CX}} \gg g$), a sharp N-photon resonance emerges with N being an integer. It corresponds to a polariton of the type $(|G,0\rangle \pm |X,N\rangle)/\sqrt{2}$, where $|\chi,n\rangle$ denotes the product state of the 2LS state $|\chi\rangle$ with $\chi \in \{G,X\}$ and the photon number state $|n\rangle$. When dissipative channels are included by introducing the excited state's radiative decay with rate γ and resonator losses with rate κ, this resonance becomes a source of N-photon bundles [27].

This mechanism is sketched in Fig. 2. Because the 2LS is strongly driven ($f \gg g$) and the dispersive regime ($\Delta\omega_{\mathrm{CX}} \gg g$) is considered, the coupling to the resonator represents a small perturbation to the driven 2LS. Thus the system is best discussed using the two eigenstates

$$|+\rangle = \alpha|G\rangle + \beta|X\rangle, \tag{3a}$$

$$|-\rangle = \beta|X\rangle - \alpha|G\rangle \tag{3b}$$

of the system Hamiltonian $H_{\rm Sys}$ without the resonator coupling, i.e., $g = 0$ in Eq. (2), which are typically referred to as the laser-dressed states. In general, the laser-dressed states are admixtures of both bares states, and the mixing coefficients $\alpha, \beta \in \mathbb{R}$ depend on the driving strength f and the detuning $\Delta\omega_{\rm LX}$. In order to create N-photon bundles, the resonator mode (in the rotating frame) is adjusted to the N-photon resonance between the lower laser-dressed state without photons $|-, 0\rangle$ and the higher laser-dressed state with N photons inside the resonator $|+, N\rangle$. The resonator introduces then an effective (Nth-order) coupling between these two states [29], which we denote as $\mathcal{V}_{\rm eff}$ in Fig. 2. In the relevant situation here, were the laser is typically strongly detuned from the 2LS, the laser-dressed states are essentially the bare states $|+\rangle \approx |X\rangle$ and $|-\rangle \approx |G\rangle$. Therefore the polariton $(|G, 0\rangle \pm |X, N\rangle)/\sqrt{2}$ is formed which corresponds to N-photon Rabi oscillations between the involved states. Dissipative channels lead to further couplings between the states $|\pm, n\rangle$, cf. schematic sketch in Fig. 2. Therefore, after the state $|+, N\rangle$ has been reached due to the effective resonator coupling, the resonator losses with rate $n\kappa$ lead to a cascaded decay. The characteristic N-photon bundle statistics is a direct result of the ratio $(n + 1)/n$ between subsequent loss rates $n\kappa$ associated with the state $|+, n\rangle$. In contrast, the radiative decay with rate γ provides a pathway from $|+, n\rangle \approx |X, n\rangle$ to $|-, n\rangle \approx |G, n\rangle$ at the same photon number.

We include both dissipative effects by accounting for the Lindblad superoperators $\mathcal{L}_{|G\rangle\langle X|,\gamma}$ and $\mathcal{L}_{a,\kappa}$ acting on the density matrix ρ as

$$\mathcal{L}_{O,\Gamma}\rho = \Gamma\left(O\rho O^\dagger - \tfrac{1}{2}\{\rho, O^\dagger O\}_+\right), \tag{4}$$

describing loss processes with rate Γ on a dissipation channel O, where $\{A, B\}_+$ is the anti-commutator of operators A and B.

The time evolution of the density matrix ρ is then governed by the Liouville-von Neumann equation

$$\frac{\partial}{\partial t}\rho = \frac{1}{i\hbar}[H, \rho]_- + \mathcal{L}_{a,\kappa}\rho + \mathcal{L}_{|G\rangle\langle X|,\gamma}\rho, \tag{5}$$

where $[A, B]_-$ is the commutator of operators A and B. In the following, we introduce two different driven 2LS-resonator systems. Depending on the considered system, the Hamilton operator H may include further contributions in addition to $H_{\rm Sys}$.

1. QD model

At first, we consider a self-assembled GaAs QD system in a single-mode microcavity. In these systems, additionally the pure-dephasing coupling of the electronic states to an environment of longitudinal acoustic phonons is important [43,44], i.e., $H = H_{\rm Sys} + H_{\rm Ph}$ in Eq. (5). It is described by the Hamiltonian [45–48]

$$H_{\rm Ph} = \hbar\sum_{\boldsymbol{q}} \omega_{\boldsymbol{q}} b_{\boldsymbol{q}}^\dagger b_{\boldsymbol{q}} + \hbar\sum_{\boldsymbol{q}} \left(\gamma_{\boldsymbol{q}}^{\rm X} b_{\boldsymbol{q}}^\dagger + \gamma_{\boldsymbol{q}}^{\rm X*} b_{\boldsymbol{q}}\right)|X\rangle\langle X|, \tag{6}$$

where $b_{\boldsymbol{q}}$ ($b_{\boldsymbol{q}}^\dagger$) annihilates (creates) a phonon of energy $\hbar\omega_{\boldsymbol{q}}$ in mode $\boldsymbol{q}$ with the coupling strength $\gamma_{\boldsymbol{q}}^{\rm X}$. The phonons are assumed to be initially in thermal equilibrium at temperature T.

This coupling to phonons is the source of many well-known effects in QDs, like the phonon sideband in the QD emission spectrum [45,49], the renormalization of the Rabi frequency [50,51], and the damping of Rabi oscillations [52–54]. It should be noted that because of the QD-phonon interaction resonances are found at different spectral positions due to the polaron shift. Whenever we refer to the excited state energy when phonons are taken into account, we mean the polaron-shifted excited state energy.

To treat this full many-body Hamiltonian in a numerically exact way, we employ an iterative real-time path-integral formalism [55–59] to solve the Liouville–von Neumann equation. Details on the used path-integral algorithm can be found in Appendix A. Within this approach, all effects mentioned above are thus taken into account.

Unless noted otherwise, we take $\hbar g = 0.02$ meV [60], $\gamma = 1$ ns^{-1}, and $\kappa = 8.5$ ns^{-1} [61]. These values, in particular, the cavity loss rate κ are realistically achievable [61]. The record in cavity quality so far is around $\kappa \approx 4$ ns^{-1} to 6 ns^{-1} [60], which means that it should be possible to achieve the value of κ chosen here with current state-of-the-art equipment with reasonable effort. Further, following Ref. [27], we set $\hbar\Delta\omega_{\rm CX} = -60\hbar g = -1.2$ meV and $\hbar f = 32\hbar g = 0.64$ meV. For the phonon coupling, standard GaAs parameters [59,62] are chosen for a QD with a radius of 3 nm.

2. Superconducting qubit model

As a second example, we consider a superconducting qubit in a microwave resonator. Here, pure dephasing is negligible. Therefore no addition to the model in Sec. II A is necessary, i.e., $H = H_{\rm Sys}$ in Eq. (5).

We use the parameter set $\hbar g = 0.079$ μeV, $\gamma = 1.54$ μs^{-1}, $\kappa = 0.29$ μs^{-1}, i.e., $\kappa \ll \gamma$, taken from Ref. [5]. Again, following Ref. [27], we choose $\hbar\Delta\omega_{\rm CX} = -60\hbar g = -4.71$ μeV and $\hbar f = 32\hbar g = 2.51$ μeV.

III. RESULTS: QD-CAVITY SYSTEM

A. Resonance landscape and $N = 2$

The resonance corresponding to an N-photon bundle is found at [27,63]

$$\Delta\omega_{\rm LX} = \frac{\sqrt{4(N^2-1)f^2 + N^2\Delta\omega_{\rm CX}^2} + \Delta\omega_{\rm CX}}{N^2 - 1} + \Delta\omega_{\rm CX}. \tag{7}$$

In this work, we focus mostly on the case $N = 2$. For the QD–cavity system, this results in a detuning value of $\hbar\Delta\omega_{\rm LX} = -0.51$ meV. Higher-order bundles with $N > 2$ can be reached by tuning the excitation to the corresponding resonance according to Eq. (7), however for the realistic set of parameters assumed here they are negligible.

To illustrate the appearing resonances, we scan the stationary probability P_n of occupying the photon number states $|n\rangle$ with the laser frequency $\omega_{\rm L}$. Figure 3 shows the corresponding results for the photon number states $|n\rangle = |1\rangle$, $|2\rangle$, and $|3\rangle$ in the QD–cavity system. Three resonance peaks emerge in

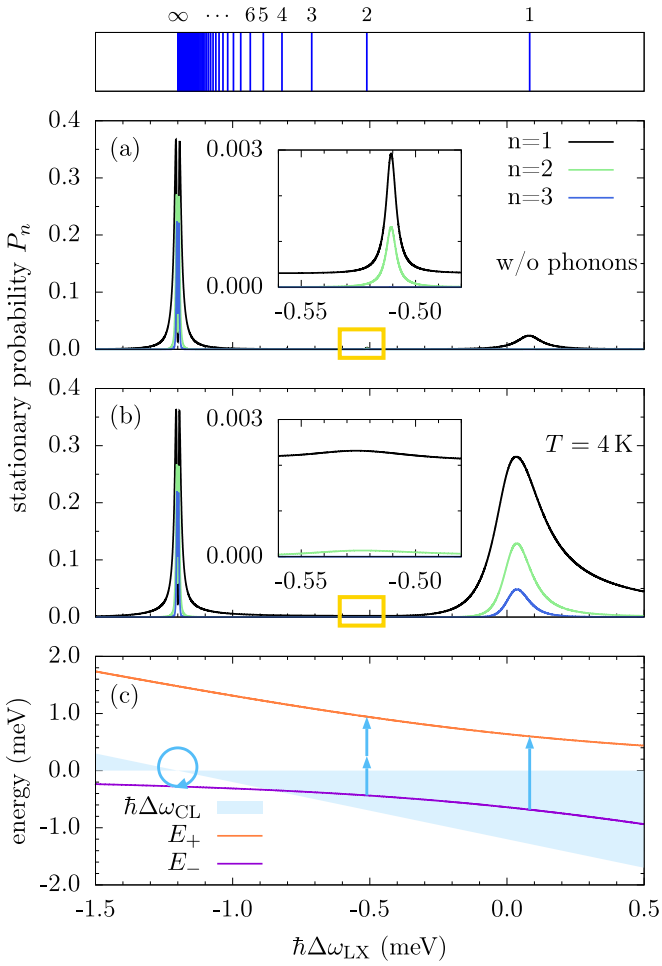

FIG. 3. Stationary probability P_n of occupying the photon number states $|n\rangle$ in the QD–cavity system as a function of the laser–exciton detuning $\Delta\omega_{\mathrm{LX}}$ (a) without taking phonon effects into account, (b) including phonons initially at $T = 4$ K (the insets show the region marked by yellow boxes on a larger scale), (c) the corresponding energies of the laser-dressed states $|+\rangle$ and $|-\rangle$. The energy of a photon in the rotating frame is given by the cavity–laser detuning $\hbar\Delta\omega_{\mathrm{CL}}$, which is plotted as a shaded area to illustrate its modulus. Arrows indicate the number of photons involved in the processes leading to the various resonance peaks, while their length corresponds to their energy $\hbar\Delta\omega_{\mathrm{CL}}$. The circular arrow indicates a one-photon process with a photon energy (in the rotating frame) of $\hbar\Delta\omega_{\mathrm{CL}} = 0$. The blue lines above panel (a) mark the energetic positions of the bundle resonances, starting for $N = 1$ and quickly converging to $\hbar\Delta\omega_{\mathrm{CX}}$ for larger N. Since the bundle resonance is derived from the condition that N cavity photons energetically fit between the two dressed states, an equation analogous to Eq. (7) can be found for the trivial case $N = 1$.

the vicinity of the bundle resonance [presented in Fig. 3(a)], which itself is shown on a magnified scale in the inset.

The most prominent peaks are found for the limiting cases $N \to \infty$ and $N = 1$. For $N \to \infty$ a double-peaked structure emerges at $\hbar\Delta\omega_{\mathrm{LX}} = \hbar\Delta\omega_{\mathrm{CX}} = -1.2$ meV (cf. Fig. 8 in Appendix B for a zoom-in). At its center the photon statistics is Poissonian and is hardly influenced by phonons [cf. Figs. 3(a) and 3(b)]. In contrast, the peak at $\hbar\Delta\omega_{\mathrm{LX}} \approx 0.08$ meV corresponds to the resonance for $N = 1$. Here, Fock

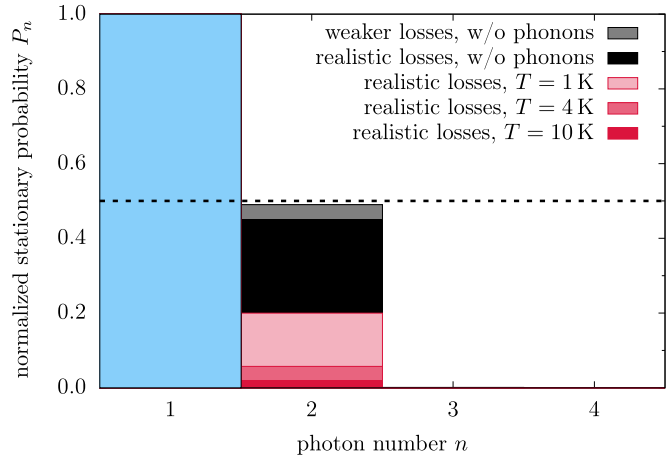

FIG. 4. The stationary probability P_n of occupying the photon number states $|n\rangle$ normalized to its value at $n = 1$ for the QD–cavity system. While the data labeled 'realistic losses' is obtained using the parameters listed in Sec. II A 1, weaker losses of $\gamma = 0.01g$ and $\kappa = 0.1g$ were chosen following Ref. [27] for the calculation shown in gray. Note that in the phonon-free case, the absolute values of the Fock state with $n = 1$ are 0.016 for the weaker losses and 0.003 for the realistic parameter set.

states with $n > 1$ are not occupied due to a photon blockade effect [cf. Fig. 3(a)], which is spoiled once phonons are considered: then, the system can climb up the Jaynes-Cummings ladder [cf. Fig. 3(b)]. The different physical mechanisms giving rise to these two limiting cases and the phonon influence on them is discussed in detail in Appendix B.

We now consider the range of bundle physics for $1 < N < \infty$ and focus on $N = 2$. The characteristic bundle statistics as denoted in Eq. (1) is well visible for the two-photon bundle shown in the inset of Fig. 3(a), in particular, the three-photon occupation probability is zero.

To understand all the resonances, we diagonalize the Hamiltonian of the laser-driven 2LS neglecting the cavity (since $f \gg g$). As a result, we obtain the laser-dressed states $|+\rangle$ and $|-\rangle$. Their energies in the laser-rotating frame are plotted in Fig. 3(c) along with the energy of a cavity photon given by $\hbar\Delta\omega_{\mathrm{CL}}$ in this frame.

The analysis in terms of laser-dressed states confirms the fact that the two-photon bundle resonance at $\hbar\Delta\omega_{\mathrm{LX}} = -0.51$ meV originates from a two-photon process [27], in this case a transition from $|-, 0\rangle$ to $|+, 2\rangle$. The study of the influence of the phonons on this resonance shows that already at 4 K [inset of Fig. 3(b)], it is strongly suppressed. The occupation probability P_1 strongly rises around the resonance peak. While the absolute value of P_1 is only weakly affected when phonons are included, the height of the peak associated with P_2 is reduced by one order of magnitude from 1.3×10^{-3} to 1.3×10^{-4}. In particular, the characteristic $1/n$ fingerprint [cf. Eq. (1)] of the number distribution is violated.

To illustrate this point in more detail, the stationary photon number distribution normalized to its value at $n = 1$ is shown in Fig. 4. First of all, it is interesting to note that the ideal bundle statistics $P_n \propto 1/n$ is only observed for loss parameters weaker than the realistic, state-of-the-art values (cf. gray data in Fig. 4). This parameter set consists of $\gamma = 0.01g =$

$0.3\ \mathrm{ns}^{-1}$ and $\kappa = 0.1g = 3\ \mathrm{ns}^{-1}$, following the values chosen in Ref. [27]. Already the slightly higher values chosen in our work in accordance with current experiments (cf. Sec. II A 1) lead to a ratio of the stationary two- to the one-photon occupation probability

$$r := \lim_{t\to\infty} \frac{\langle |2\rangle\langle 2|\rangle(t)}{\langle |1\rangle\langle 1|\rangle(t)} = \lim_{t\to\infty} \frac{P_2(t)}{P_1(t)} \tag{8}$$

equal to 0.45. Thus the ratio deviates from the target of 0.50, which is a necessary indicator for an $N = 2$ bundle. The phonon coupling pushes this value down to $r = 0.20$ already at $T = 1$ K. For higher temperatures up to 10 K, r swiftly approaches zero and the two-photon bundle fingerprint cannot be observed anymore. The N-photon bundle statistics ($1 < N < \infty$) therefore seems to be hard to find in state-of-the-art QD–cavity systems.

The reason for the drastic phonon influence can be understood by revisiting Fig. 2. Besides the effective two-photon process (blue arrows) creating the bundle, the coupling to the cavity also introduces one-photon processes between $|\pm, n\rangle$ and $|\pm, n+1\rangle$. In the phonon-free situation, these processes are strongly detuned from the cavity mode, and therefore highly unlikely to occur. But when LA phonons are considered, the energetic mismatch can be compensated by a simultaneous phonon emission. Note that phonon emission is possible at any temperature and always dominates over phonon absorption. The phonon-assisted one-photon transitions from $|-, 0\rangle$ to $|-, 1\rangle$ are competing against the two-photon bundle process (blue arrows). This competing second-order process, where one photon and one phonon are emitted simultaneously dominates over the bundle mechanisms. After the state $|-, 1\rangle$ is reached due to the phonon-assisted one-photon transitions, the cavity losses direct the system back to state $|-, 0\rangle$, provided that the cavity loss rate is larger than the phonon-assisted coupling towards further states $|-, n\rangle$ with $n > 1$. Consequently, the system just transitions back and forth between these two states, resulting in a suppressed two-photon occupation probability and a violation of the bundle statistics. With increasing temperature, phonon-assisted processes gain importance, resulting in an even stronger suppression of the bundle.

Our finding that due to the phonon influence the occupation probability P_2 of the $n = 2$ Fock state compared with the $n = 1$ state is much lower than expected for an $N = 2$ bundle does, however, not mean that two-photon emission features are precluded from observation. The latter can still be made prominent, e.g., by spectrally filtering the emission as has been shown in Ref. [29].

B. Comparison with a phenomenological dephasing model

The phonon environment has a drastic influence on the N-photon bundle statistics as shown in the previous section for the case $N = 2$. Already at a low temperature of $T = 1$ K the $1/n$-distribution characteristic for the bundle [cf. Eq. (1)] is not recognizable anymore (cf. Fig. 4). This result was obtained within a microscopic model of the phonon influence. In contrast, in Ref. [27], the dephasing has been analyzed using a phenomenological Lindblad operator $\mathcal{L}_{|X\rangle\langle X|,\gamma_\phi}$.

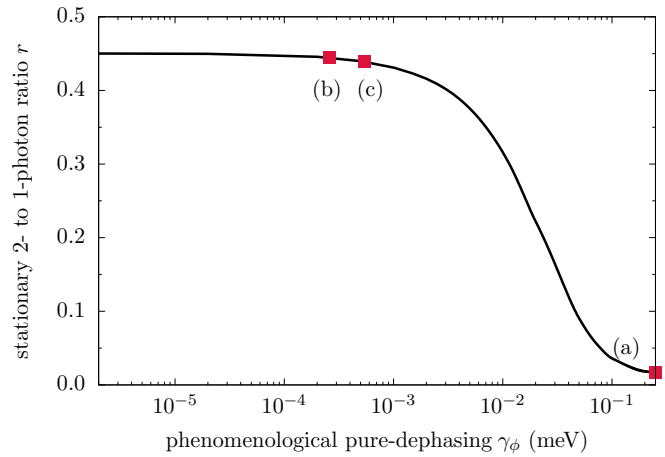

FIG. 5. The stationary ratio between the two- and the one-photon occupation probability in the QD–cavity system with the phonon influence approximated by a Lindblad operator with a phenomenological pure dephasing rate γ_ϕ instead of the microscopic Hamiltonian H_{Ph} in Eq. (6), cf. main text. (a) γ_ϕ corresponding to the full driven Jaynes–Cummings model at $T = 4$ K. (b) γ_ϕ corresponding to a Jaynes–Cummings dynamics with $n = 1$. (c) γ_ϕ corresponding to a Jaynes–Cummings dynamics with $n = 2$.

It is therefore instructive to compare the microscopic model with the phenomenological one to check whether the latter is valid. On first sight, we find a quite different behavior: for the phenomenological model taking values for the corresponding Lindblad rate γ_ϕ from the literature on semiconductor QD-cavity systems, the impact of pure dephasing is almost negligible [27].

To analyze this in more detail, we have plotted results of the phenomenological model in Fig. 5, which shows the stationary ratio r as a function of the phenomenological pure-dephasing rate γ_ϕ which is incorporated into the model by the addition of the Lindblad operator $\mathcal{L}_{|X\rangle\langle X|,\gamma_\phi}$ instead of the microscopic Hamiltonian model H_{Ph}. Indeed, in that approximation a large plateau range is found where the ratio stays essentially at its phonon-free value of $r = 0.45$ (cf. also Fig. 4).

To assess, what γ_ϕ should be chosen in the reduced model to best approximate the full phonon effect, we apply the following procedure: We compare the exciton dynamics resulting from the full calculation (where phonons are included by H_{Ph}) with the phenomenological model (where H_{Ph} is replaced by $\mathcal{L}_{|X\rangle\langle X|,\gamma_\phi}$) and vary γ_ϕ until the envelopes of the two dynamical results essentially match. Note that we set $\kappa = \gamma = 0$ for this procedure to extract the pure phonon influence on the dynamics. Furthermore, this comparison is conducted for the all-resonant case, i.e., $\Delta\omega_{\mathrm{LX}} = \Delta\omega_{\mathrm{CX}} = 0$. We perform this procedure at $T = 4$ K for three different cases and mark the resulting rate γ_ϕ by red squares in Fig. 5. (a) Driven Jaynes-Cummings system with the initial state $|G, 0\rangle$, resembling the closest approximation to the full calculation, (b) Jaynes-Cummings system without driving ($f = 0$) for the initial state $|G, 1\rangle$, and (c) same as (b) but with $|G, 2\rangle$ as the initial state. The three extracted rates (cf. Fig. 5) indicate that a very large pure-dephasing rate of the order of 10^{-1} meV is necessary to reproduce the dynamics of the full microscopic model [cf. red

square labeled with (a)]. With such a large rate, the ratio r is close to zero, meaning that no two-photon bundle statistics is observed in accordance with the results of the full model at $T = 4$ K (cf. Fig. 4).

The reason for such a significant increase in γ_ϕ lies in the impact of the pure dephasing mechanism, which gains in strength for larger Rabi frequencies related to the effective couplings present in the system. While in (b) and (c) the cavity Rabi frequency amounts to $2g\sqrt{n+1}$ with n the number of photons present in the cavity, the driving $f \gg g$ introduces the highest transition frequency in (a). In Fig. 5, it becomes clear that the pure-dephasing rate increases with larger effective coupling, in accordance with earlier observations in the case of a microscopic description of phonons [53,64,65]. The values of γ_ϕ in (b) and (c) are of the order of experimentally found pure-dephasing rates for strong QD-cavity coupling like the one studied here (cf. Sec. II A 1), but without external driving. Choosing such values for the rate indeed results in a marginal influence of pure dephasing, since both points lie well inside the plateau region.

Thus the conclusion in Ref. [27] that dephasing does not significantly affect the N-photon bundle generation can be traced back to the fact that values for dephasing rates have been considered that are no longer applicable in the regime of very strong driving as required for this protocol. The physical reason lies in the fact that an optically driven system is influenced by the phonon Hamiltonian in a profoundly different way than its nondriven counterpart: while phonons cannot induce transitions between the two electronic states in the undriven case, they can lead to transitions between the laser-dressed states, which are the eigenstates of the driven two-level system [66]. In essence, the dephasing rate depends on the driving strength. A quadratic dependence $\gamma_\phi \propto f^2$ can be derived in a weak-coupling limit [67].

In conclusion, a phenomenological pure dephasing model is also able to qualitatively predict that the characteristic statistical fingerprint of N-photon bundles is violated. The challenge is the choice of a proper rate, which has to be calibrated to the full phonon system. Since non-Markovian features are missing in the phenomenological model our results indicate that, in the present case, non-Markovian effetcs are of minor importance and, indeed, phonon-induced tranitions between laser dressed states are the origin of the violation of the bundle statistics.

IV. RESULTS: SUPERCONDUCTING QUBIT-MICROWAVE RESONATOR SYSTEMS

Superconducting qubit–microwave resonator systems have been successfully used to demonstrate the on-demand preparation of various highly nonclassical photon states, such as Fock states [4], superpositions thereof, and Voodoo cat states, i.e., coherent superpositions of three coherent states [5]. In none of these experiments, a significant impact of pure dephasing was reported.

For state-of-the-art superconducting systems [5], the resonator losses are much smaller than the decay of the qubit ($\kappa \ll \gamma$ as in Sec. II A 2). Again, the two-photon bundle resonance is achieved by an external excitation tuned according to Eq. (7). The resulting photon number distribution is shown in Fig. 6, normalized to its value at $n = 1$ (light blue bars). No bundle statistics is found, as higher order photon number states can be reached. Consequently, the characteristic cutoff for $n > N = 2$ is not observed.

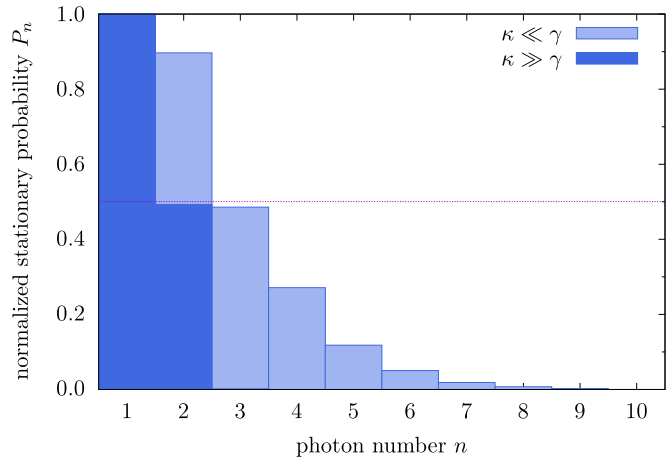

FIG. 6. The stationary probability P_n of occupying the photon number states $|n\rangle$ normalized to its value at $n = 1$ for the superconducting qubit–microwave system. The data labeled $\kappa \ll \gamma$ is obtained using the parameters from Sec. II A 2. In dark blue, the result of a calculation with a cavity loss rate two orders of magnitude larger than in Sec. II A 2 is shown, namely $\kappa = 0.1g = 7.76\gamma$, cf. Fig. 4.

The reason for this finding lies in the fact that the radiative decay with rate γ can induce transitions from states $|+, n\rangle$ to $|-, n\rangle$, as indicated in Fig. 2. After the state $|+, N\rangle$ is reached due to the N-photon resonance in the bundle-mechanism, these radiative transitions represent a competing channel in addition to the cascaded decay caused by the resonator losses. If at any point in the subsequent cascade, the radiative decay rate γ becomes comparable to the resonator loss rate $n\kappa$ ($n \leqslant N$) associated with the state $|+, n\rangle$, the system can reach the state $|-, n\rangle$. Because the coupling to the resonator does not only induce an effective coupling between the states $|-, 0\rangle$ and $|+, N\rangle$, but between all pairs $|-, n\rangle$ and $|+, n + N\rangle$, cf. Fig. 2, a subsequent emission of N additional resonator photons is possible when the system transitions into the state $|+, n + N\rangle$. Consequently, the characteristic cutoff is lost and higher order Fock states can be reached, violating the bundle-statistics.

This interpretation is supported by Fig. 6. For $n = 5$, the resonator loss rate $n\kappa$ becomes comparable to γ. Thus the last significant two-photon emission occurs due to the transition from $|-, 5\rangle$ to $|+, 7\rangle$. Afterwards the resonator losses dominate and the stationary probabilities P_n essentially vanish for $n > 7$.

Thus the failure of the superconducting qubit to show the statistical fingerprint can be traced back to the lack of resonator losses κ in comparison to radiative decay γ. Indeed, if we consider a resonator loss rate much larger (following Ref. [27], $\kappa = 0.1g$ has been chosen, cf. also Fig. 4 for this specific choice), we can obtain a near-perfect two-photon bundle statistics. The resulting photon number distribution (cf. dark blue bars in Fig. 6) indeed shows a near-perfect two-photon bundle fingerprint, with $r = 0.49$ and no occupation

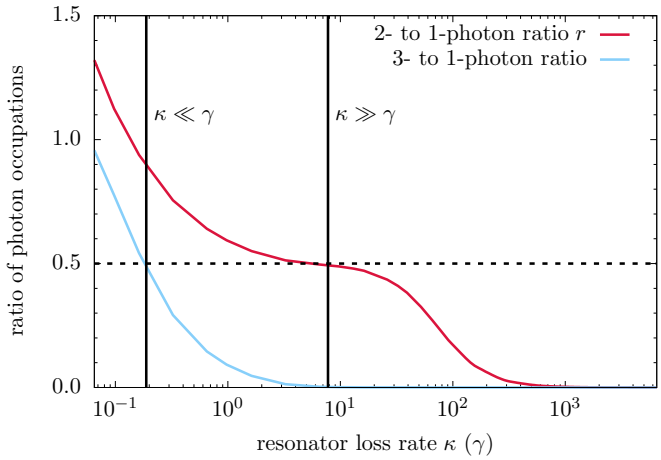

FIG. 7. The stationary ratios of the two- to one-photon occupation probabilities and of the three- to one-photon occupation probabilities as functions of the resonator loss rate κ (in units of γ) for the superconducting qubit–microwave system. The two vertical black lines mark those values of κ, which are used to obtain the corresponding data in Fig. 6. The dotted black line shows the target value of 0.5 for the ratio r.

probability for $n > 2$. This means that though much effort is usually invested into resonators of better quality, here the use of a bad resonator is mandatory.

To analyze the impact of the losses in more detail, we study the bundle statistics as a function of the resonator losses. To this end, the two- to one-photon ratio r is shown as a function of κ in Fig. 7 as well as the three- to one-photon ratio, which should vanish for an ideal two-photon bundle emission due to the cutoff for $n > N = 2$. Indeed, these two quantities confirm that the chosen value of $\kappa = 0.1g = 7.76\gamma$ lies well within a plateau region of $r \approx 0.5$ and a vanishing occupation probability for $n > 2$. While resonator losses too low compared to the decay of the qubit result in the occupation of states with $n > 2$, using very low-quality resonators with $\kappa \gtrsim 20\gamma$ (cf. Fig. 7) leads to a drastic reduction of r and thus a photon statistics, which displays a two-photon component much smaller than the ideal two-photon bundle. While constructing resonators of better quality is always an experimental challenge, creating a resonator of intermediate quality should be a lesser problem. Thus superconducting qubit-microwave resonator systems are indeed suitable candidates for sources of N-photon bundles, in agreement with Ref. [68].

V. CONCLUSION

We have studied the N-photon bundle statistics in two solid-state platforms: semiconductor quantum-dot–cavity systems and superconducting qubit-microwave resonator systems.

In quantum-dot–cavity systems, pure dephasing is induced by longitudinal acoustic phonons. We have found that even at low operating temperatures of a few kelvin, the characteristic bundle statistics [cf. Eq. (1)] cannot prevail for $N = 2$, thereby implying that a corresponding statistics for $N > 2$ is also out of reach with current state-of-the-art samples. The reason is the considered driving regime that is required to address the bundle resonance, which also favors the phonon activity in the electronic subsystem of the quantum dot.

In contrast, superconducting qubit–microwave resonator systems are suitable candidates for the observation of the N-photon bundle statistics. Here, the pure dephasing does not play a notable role. However, the quality of the resonator has to be in a certain, optimal range. In particular, it should not be too high to facilitate the emission of photon bundles.

ACKNOWLEDGMENTS

This work was funded by the Deutsche Forschungsgemeinschaft (DFG, German Research Foundation), Project No. 419036043.

APPENDIX A: ITERATIVE REAL-TIME PATH-INTEGRAL ALGORITHM

In this section, a brief description of the iterative real-time path-integral algorithm is given. This formalism is used to obtain the time evolution of the reduced density matrix $\bar{\rho}$ for the system of interest, i.e., the driven QD-cavity system, which is coupled to LA phonons via the pure-dephasing type Hamiltonian H_{Ph}.

The time evolution of the full statistical operator ρ of the system, containing all QD, photonic and phonon degrees of freedom, is governed by the Liouville-von Neumann equation

$$\frac{\partial}{\partial t}\rho = \mathcal{L}_{\mathrm{Sys}}\rho + \mathcal{L}_{\mathrm{Ph}}\rho, \tag{A1a}$$

$$\mathcal{L}_{\mathrm{Sys}}\rho = \frac{1}{i\hbar}[H_{\mathrm{Sys}}, \rho]_- + \mathcal{L}_{a,\kappa}\rho + \mathcal{L}_{|G\rangle\langle X|,\gamma}\rho, \tag{A1b}$$

$$\mathcal{L}_{\mathrm{Ph}}\rho = \frac{1}{i\hbar}[H_{\mathrm{Ph}}, \rho]_-. \tag{A1c}$$

First, a basis of ket states $|\mu\rangle$ and corresponding bra states $\langle\nu|$ for the system of interest is introduced. In the situation studied here, the basis $|\mu\rangle$ comprises the states $|G, n\rangle$, $|X, n\rangle$ with $n \leqslant N_{\max} \in \mathbb{N}_0$, where $N_{\max}$ is the maximum number of cavity photons that are considered in our numerical simulations. The reduced density matrix $\bar{\rho} = \mathrm{Tr}_{\mathrm{Ph}}[\rho]$, which is obtained from the statistical operator of the complete system by performing the trace over the phonon degrees of freedom can be expressed in the basis of the driven QD-cavity system as

$$\bar{\rho} = \sum_{\nu,\mu} \bar{\rho}_{\nu\mu}\, |\nu\rangle\langle\mu|, \tag{A2a}$$

$$\bar{\rho}_{\nu\mu} = \langle\nu|\mathrm{Tr}_{\mathrm{Ph}}[\rho]|\mu\rangle. \tag{A2b}$$

In Ref. [55], it was demonstrated that when the system dynamics is Hamiltonian, $\bar{\rho}_{\nu\mu}$ can be expressed as a sum over paths that can be performed iteratively, without introducing further approximations to the model. Furthermore, it has been shown recently that this still holds when non-Hamiltonian contributions to $\mathcal{L}_{\mathrm{Sys}}$ are taken into account, as provided, e.g., by $\mathcal{L}_{a,\kappa}$ and $\mathcal{L}_{|G\rangle\langle X|,\gamma}$ [58].

The general idea is to rewrite the formal solution of Eq. (A1a) by discretizing the time-evolution operator into small steps and integrating over the phonon degrees of freedom. When an equally spaced time discretization $t_\ell = \Delta t\ \ell$

with time step Δt and $\ell \in \mathbb{N}_0$ as well as a finite memory length $t_m = n_m \Delta t$ is considered, and the states of the driven QD-cavity system at time t_ℓ are labeled by ν_ℓ or μ_ℓ, the reduced density matrix at time t_n is given by

$$\bar{\rho}_{\nu_n \mu_n}(t_n) = \sum_{\substack{\nu_{n-1}\ldots\nu_{n-n_m+1} \\ \mu_{n-1}\ldots\mu_{n-n_m+1}}} \rho^{\mu_n \ldots \mu_{n-n_m+1}}_{\nu_n \ldots \nu_{n-n_m+1}}. \tag{A3}$$

The so called *augmented density matrix* (ADM) [55,56] $\rho^{\mu_n \ldots \mu_{n-n_m+1}}_{\nu_n \ldots \nu_{n-n_m+1}} := \sum_{\substack{\nu_{n-n_m}\ldots\nu_0 \\ \mu_{n-n_m}\ldots\mu_0}} R^{\mu_n \ldots \mu_0}_{\nu_n \ldots \nu_0}$ obeys the recurrence [58]

$$\rho^{\mu_n \ldots \mu_{n-n_m+1}}_{\nu_n \ldots \nu_{n-n_m+1}} = \mathcal{M}^{\nu_{n-1}\mu_{n-1}}_{\nu_n \mu_n} \sum_{\substack{\nu_{n-n_m} \\ \mu_{n-n_m}}} \exp\left(\sum_{\ell=n-n_m}^{n} S^{\nu_\ell \mu_\ell}_{\nu_n \mu_n} \right) \rho^{\mu_{n-1}\ldots\mu_{n-n_m}}_{\nu_{n-1}\ldots\nu_{n-n_m}}, \tag{A4}$$

where

$$\mathcal{M}^{\nu_{\ell-1}\mu_{\ell-1}}_{\nu_\ell \mu_\ell} = \langle \nu_\ell | \, \mathcal{M}_{t_{\ell-1},t_\ell}[|\nu_{\ell-1}\rangle\langle\mu_{\ell-1}|] \, |\mu_\ell\rangle, \tag{A5a}$$

$$\mathcal{M}_{t,t'}[\cdot] = \mathcal{T} \exp\left(\int_t^{t'} \mathcal{L}_{\mathrm{Sys}} \, dt'' \right)[\,\cdot\,], \tag{A5b}$$

$$R^{\mu_n \ldots \mu_0}_{\nu_n \ldots \nu_0} := \bar{\rho}_{\nu_0 \mu_0} \prod_{\ell=1}^{n} \mathcal{M}^{\nu_{\ell-1}\mu_{\ell-1}}_{\nu_\ell \mu_\ell} \exp\left(\sum_{\ell=1}^{n} \sum_{\ell'=1}^{\ell} S^{\nu_{\ell'}\mu_{\ell'}}_{\nu_\ell \mu_\ell} \right). \tag{A5c}$$

Here it is assumed that initially the system is in its ground state $|G, 0\rangle$ while the phonons are in a thermal equilibrium at temperature T. The influence of the phonons is captured in the functions $S^{\nu_{\ell'}\mu_{\ell'}}_{\nu_\ell \mu_\ell}$, which introduce a finite memory.

For the pure-dephasing type Hamiltonian H_{Ph} with real couplings $\gamma^{\mathrm{X}}_{\boldsymbol{q}}$, the explicit expressions for these functions are [57,59]

$$S^{\nu_{\ell'}\mu_{\ell'}}_{\nu_\ell \mu_\ell} = -K_{\nu_{\ell'}\nu_\ell}(t_\ell - t_{\ell'}) - K^*_{\mu_\ell \mu_{\ell'}}(t_\ell - t_{\ell'}) + K^*_{\nu_\ell \mu_{\ell'}}(t_\ell - t_{\ell'}) + K_{\nu_{\ell'}\mu_\ell}(t_\ell - t_{\ell'}), \tag{A6a}$$

$$K_{\nu_\ell \mu_{\ell'}}(\tau) = 2 \int_0^\infty d\omega \frac{J_{\nu_\ell \mu_{\ell'}}(\omega)}{\omega^2} [1 - \cos(\omega \Delta t)] \left[\coth\left(\frac{\hbar\omega}{2k_B T} \right) \cos(\omega\tau) - i \sin(\omega\tau) \right], \quad \tau > 0 \tag{A6b}$$

$$K_{\nu_\ell \mu_\ell}(0) = \int_0^\infty d\omega \frac{J_{\nu_\ell \mu_\ell}(\omega)}{\omega^2} \left[\coth\left(\frac{\hbar\omega}{2k_B T} \right) (1 - \cos(\omega \Delta t)) + i \sin(\omega \Delta t) - i\omega \Delta t \right], \tag{A6c}$$

$$J_{\nu\mu}(\omega) = \sum_{\boldsymbol{q}} \gamma^{\nu}_{\boldsymbol{q}} \gamma^{\mu *}_{\boldsymbol{q}} \delta(\omega - \omega_{\boldsymbol{q}}); \quad \text{with } \gamma^{\nu}_{\boldsymbol{q}} = n_\nu \gamma^{\mathrm{X}}_{\boldsymbol{q}}. \tag{A6d}$$

They display two important properties. (i) In the case of a continuum of phonon modes, the induced memory is finite, i.e., the memory kernel $K_{\nu_\ell \mu_{\ell'}}(t_\ell - t_{\ell'})$, and in turn $S^{\nu_{\ell'}\mu_{\ell'}}_{\nu_\ell \mu_\ell}$, become negligibly small for $t_\ell - t_{\ell'} > t_m = n_m \Delta t$. This property is already exploited in the recurrence Eq. (A4), where it is sufficient to memorize only the past n_m time steps to calculate the next one.

(ii) The function $S^{\nu_{\ell'}\mu_{\ell'}}_{\nu_\ell \mu_\ell}$ depends on the indices $\nu_\ell, \mu_\ell, \nu_{\ell'}, \mu_{\ell'}$ solely via the *phonon spectral density* $J_{\nu\mu}(\omega)$ and its dependence on the corresponding couplings $\gamma^{\nu}_{\boldsymbol{q}} = n_\nu \gamma^{\mathrm{X}}_{\boldsymbol{q}}$, where $n_\nu \in \{0, 1\}$ is the number of excitons present in the QD-cavity state $|\nu\rangle$. This property is exploited in an advanced algorithm, that was first introduced in the supplement of Ref. [59].

The central idea is to divide the QD-cavity states $|\nu\rangle$ into groups where each member couples identically to the phonon degrees of freedom. In the situation considered here, the coupling to the LA phonons depends solely on the QD state. Thus the states $|\nu\rangle$ can be sorted into two groups $\{|G, n\rangle\}$ and $\{|X, n\rangle\}$. Formally, the states can be re-labeled $|\nu\rangle \to |\lambda, k\rangle$ and $|\mu\rangle \to |\bar{\lambda}, \bar{k}\rangle$, where $\lambda \in \{1, 2\}$ denotes the group and k distinguishes the different members within this group. After defining the *partially summed ADM* (PSADM)

$$\rho^{(\bar{\lambda}_n, \bar{k}_n)\bar{\lambda}_{n-1}\ldots\bar{\lambda}_{n-n_m+1}}_{(\lambda_n, k_n)\lambda_{n-1}\ldots\lambda_{n-n_m+1}} := \sum_{\substack{k_{n-1}\ldots k_{n-n_m+1} \\ \bar{k}_{n-1}\ldots\bar{k}_{n-n_m+1}}} \rho^{(\bar{\lambda}_n, \bar{k}_n)(\bar{\lambda}_{n-1}, \bar{k}_{n-1})\ldots(\bar{\lambda}_{n-n_m+1}, \bar{k}_{n-n_m+1})}_{(\lambda_n, k_n)(\lambda_{n-1}, k_{n-1})\ldots(\lambda_{n-n_m+1}, k_{n-n_m+1})}. \tag{A7}$$

One obtains the recursion relation [59]

$$\rho^{(\bar{\lambda}_n, \bar{k}_n)\bar{\lambda}_{n-1}\ldots\bar{\lambda}_{n-n_m+1}}_{(\lambda_n, k_n)\lambda_{n-1}\ldots\lambda_{n-n_m+1}} = \sum_{\substack{k_{n-1} \\ \bar{k}_{n-1}}} \mathcal{M}^{(\lambda_{n-1}, k_{n-1})(\bar{\lambda}_{n-1}, \bar{k}_{n-1})}_{(\lambda_n, k_n)(\bar{\lambda}_n, \bar{k}_n)} \sum_{\substack{\lambda_{n-n_m} \\ \bar{\lambda}_{n-n_m}}} \exp\left(\sum_{\ell=n-n_m}^{n} S^{\lambda_\ell \bar{\lambda}_\ell}_{\lambda_n \bar{\lambda}_n} \right) \rho^{(\bar{\lambda}_{n-1}, \bar{k}_{n-1})\bar{\lambda}_{n-2}\ldots\bar{\lambda}_{n-n_m}}_{(\lambda_{n-1}, k_{n-1})\lambda_{n-2}\ldots\lambda_{n-n_m}} \tag{A8}$$

for this quantity. Then, the reduced density matrix for the driven QD-cavity system at time t_n is given by

$$\bar{\rho}_{\nu_n \mu_n}(t_n) = \sum_{\substack{\lambda_{n-1}\ldots\lambda_{n-n_m+1} \\ \bar{\lambda}_{n-1}\ldots\bar{\lambda}_{n-n_m+1}}} \rho^{(\bar{\lambda}_n, \bar{k}_n)\bar{\lambda}_{n-1}\ldots\bar{\lambda}_{n-n_m+1}}_{(\lambda_n, k_n)\lambda_{n-1}\ldots\lambda_{n-n_m+1}}. \tag{A9}$$

Equations (A7)–(A9) represent an exact reformulation without any additional approximation to the model. Numerical errors can be caused either by the number of considered photons per QD state $N_{\max}$ or by two intrinsic parameters of the path-integral algorithm: (i) The finite time step Δt and (ii)

the truncation of the memory to t_m. Usually, these convergence parameters can be well controlled. A simulation is considered to be *numerically complete* if neither a further reduction of Δt nor a further increase of t_m or $N_{\max}$ changes the numerical results noticeably.

An explicit expression for the phonon spectral density $J_{\nu\mu}(\omega)$ and the material parameters used in the simulations can be found in the supplement of Ref. [59]. Typically, calculations at low temperatures are most demanding, since they require the longest memory length [57]. For the calculations at a temperature of $T = 1$ K performed in the main text, numerically complete simulations were obtained for the parameter set: $\Delta t = 0.65$ ps, $n_m = 9$, and $N_{\max} = 4$. Note that, for this set of parameters, the advanced algorithm based on the PSADM reduces the number of terms to be iterated from $N_{\mathrm{ADM}} = 10^{2n_m} \approx 1.0 \times 10^{18}$ for the full ADM to $N_{\mathrm{PSADM}} = 10^2 \cdot 2^{2(n_m-1)} \approx 6.6 \times 10^6$ [59]. Thus this reduction of the numerical demand by more than 11 orders of magnitude is the reason that a numerically complete investigation of the considered system of interest becomes feasible at all. However, it is indeed the numerically complete treatment of the microscopic model that enables us to make a judgment on the phonon influence on the bundle statistics without prejudice.

APPENDIX B: RESONANCE PEAKS FOR $N \to \infty$ AND $N = 1$

Since the peaks at $\hbar\Delta\omega_{\mathrm{LX}} = -1.2$ meV and 0.08 meV are the most striking features in Fig. 3, we shall discuss them in some detail in this Appendix. This will give additional insights into the physics taking place in this parameter regime in general, although the analysis reveals that these peaks are not related to the bundles which are the main target of our paper. The most prominent peak in Fig. 3 at $\hbar\Delta\omega_{\mathrm{LX}} = \hbar\Delta\omega_{\mathrm{CX}} = -1.2$ meV is obtained in the limit $N \to \infty$ and corresponds to a process where the photon energy in a frame rotating with the laser frequency is $\hbar\Delta\omega_{\mathrm{CL}} = 0$ and the system can climb up the photon ladder from $|-, n\rangle$ to $|-, n+1\rangle$, such that a Poissonian distribution with respect to n emerges. Note that one observes a double-peaked structure at this resonance in Fig. 3. At its center, the order of the photon occupation probabilities is reversed, i.e., the occupation probability of $n = 2$ is higher than that of $n = 1$, consistent with a Poissonian with an average photon number of $\langle n\rangle = 6.6$ and a maximum occupation probability of 0.15 at $n = 6$. A magnification of this peak, where the reversal of the photon order is visible, is replotted in Fig. 8. An analysis of the corresponding Wigner function [5,26] (not shown here) confirms that the corresponding state is a (Glauber) coherent state.

The peak at $\hbar\Delta\omega_{\mathrm{LX}} \approx 0.08$ meV corresponds to a one-photon bundle resonance, i.e., a one-photon Fock state, and also results from a one-photon process. But in contrast to the previously discussed case, the photon is emitted only by the transition from $|-, 0\rangle$ to $|+, 1\rangle$. Due to an energy mismatch between the photon energy and the transition between $|+, 1\rangle$ and $|\pm, 2\rangle$, no further photons are put into the cavity, as can be seen in the stationary probabilities P_n of occupying the photon number states $|n\rangle$ at this peak in Fig. 3(a). This effect is commonly known as the photon blockade [69].

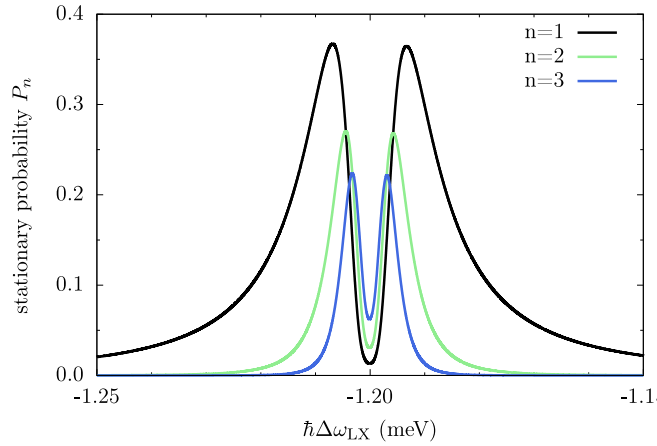

FIG. 8. Stationary probability P_n of occupying the photon number states $|n\rangle$ in the QD–cavity system as a function of the laser-exciton detuning $\Delta\omega_{\mathrm{LX}}$ without taking phonon effects into account. This is a magnification of the resonance peak for $N \to \infty$ in Fig. 3(a). On this scale, the double-peak structure and the reversal of the photon order at its center are well visible.

The phonon influence on the stationary probability P_n of occupying the photon number states $|n\rangle$ at $T = 4$ K as shown in Fig. 3(b) could not be more different for these two resonances. The first one for $N \to \infty$ at $\hbar\Delta\omega_{\mathrm{LX}} = -1.2$ meV is hardly influenced by phonons at all. Indeed, the photon number distribution remains Poissonian with a slightly lower average photon number of $\langle n\rangle = 5.6$ and a similar maximum occupation probability of 0.16 at $n = 5$. The reason lies in the fact that the photons are emitted from transitions, where the electronic (laser-dressed) state remains $|-\rangle$ and does not change. Since this is the energetically lower dressed state and at temperatures below a few tens of kelvins phonon absorption is highly unlikely, phonons have only a slight influence on the stationary photon distribution.

On the other hand, the second peak at $\hbar\Delta\omega_{\mathrm{LX}} \approx 0.08$ meV for $N = 1$ experiences strong phonon enhancement, since the photon blockade is spoiled. The energy mismatch between $|+, n\rangle$ and $|-, n\rangle$ is now bridged by phonon emission, which is possible for all temperatures down to absolute zero, and a subsequent resonant transition to $|+, n+1\rangle$ can take place. Therefore the phonon coupling drives the occupation probability of higher-order Fock states beyond $n = 1$ [59,70].

[1] F. W. Cummings and A. K. Rajagopal, Production of number states of the electomagnetic field, Phys. Rev. A **39**, 3414 (1989).

[2] B. T. H. Varcoe, S. Brattke, M. Weidinger, and H. Walther, Preparing pure photon number states of the radiation field, Nature (London) **403**, 743 (2000).

[3] X. Zhou, I. Dotsenko, B. Peaudecerf, T. Rybarczyk, C. Sayrin, S. Gleyzes, J. M. Raimond, M. Brune, and S. Haroche, Field Locked to a Fock State by Quantum Feedback with Single Photon Corrections, Phys. Rev. Lett. **108**, 243602 (2012).

[4] M. Hofheinz, E. M. Weig, M. Ansmann, R. C. Bialczak, E. Lucero, M. Neeley, A. D. O'Connell, H. Wang, J. M. Martinis,

and A. N. Cleland, Generation of Fock states in a superconducting quantum circuit, Nature (London) **454**, 310 (2008).

[5] M. Hofheinz, H. Wang, M. Ansmann, R. C. Bialczak, E. Lucero, M. Neeley, A. D. O'Connell, D. Sank, J. Wenner, J. M. Martinis, and A. N. Cleland, Synthesizing arbitrary quantum states in a superconducting resonator, Nature (London) **459**, 546 (2009).

[6] P. Michler, A. Kiraz, C. Becher, W. V. Schoenfeld, P. M. Petroff, L. Zhang, E. Hu, and A. Imamoglu, A quantum dot single-photon turnstile device, Science **290**, 2282 (2000).

[7] C. Santori, M. Pelton, G. Solomon, Y. Dale, and Y. Yamamoto, Triggered Single Photons from a Quantum Dot, Phys. Rev. Lett. **86**, 1502 (2001).

[8] C. Santori, D. Fattal, J. Vuckovic, G. S. Solomon, and Y. Yamamoto, Indistinguishable photons from a single-photon device, Nature (London) **419**, 594 (2002).

[9] Y.-M. He, Y. He, Y.-J. Wei, D. Wu, M. Atatüre, C. Schneider, S. Höfling, M. Kamp, C.-Y. Lu, and J.-W. Pan, On-demand semiconductor single-photon source with near-unity indistinguishability, Nat. Nanotechnol. **8**, 213 (2013).

[10] Y.-J. Wei, Y.-M. He, M.-C. Chen, Y.-N. Hu, Y. He, D. Wu, C. Schneider, M. Kamp, S. Höfling, C.-Y. Lu, and J.-W. Pan, Deterministic and robust generation of single photons from a single quantum dot with 99.5% indistinguishability using adiabatic rapid passage, Nano Lett. **14**, 6515 (2014).

[11] X. Ding, Y. He, Z.-C. Duan, N. Gregersen, M.-C. Chen, S. Unsleber, S. Maier, C. Schneider, M. Kamp, S. Höfling, C.-Y. Lu, and J.-W. Pan, On-Demand Single Photons with High Extraction Efficiency and Near-Unity Indistinguishability from a Resonantly Driven Quantum Dot in a Micropillar, Phys. Rev. Lett. **116**, 020401 (2016).

[12] N. Somaschi, V. Giesz, L. De Santis, J. C. Loredo, M. P. Almeida, G. Hornecker, S. L. Portalupi, T. Grange, C. Antón, J. Demory, C. Gómez, I. Sagnes, N. D. Lanzillotti-Kimura, A. Lemaítre, A. Auffeves, A. G. White, L. Lanco, and P. Senellart, Near-optimal single-photon sources in the solid state, Nat. Photonics **10**, 340 (2016).

[13] L. Schweickert, K. D. Jöns, K. D. Zeuner, S. F. Covre da Silva, H. Huang, T. Lettner, M. Reindl, J. Zichi, R. Trotta, A. Rastelli, and V. Zwiller, On-demand generation of background-free single photons from a solid-state source, Appl. Phys. Lett. **112**, 093106 (2018).

[14] L. Hanschke, K. A. Fischer, S. Appel, D. Lukin, J. Wierzbowski, S. Sun, R. Trivedi, J. Vučković, J. J. Finley, and K. Müller, Quantum dot single-photon sources with ultra-low multi-photon probability, npj Quantum Inf. **4**, 43 (2018).

[15] M. Cosacchi, F. Ungar, M. Cygorek, A. Vagov, and V. M. Axt, Emission-Frequency Separated High Quality Single-Photon Sources Enabled by Phonons, Phys. Rev. Lett. **123**, 017403 (2019).

[16] N. Akopian, N. H. Lindner, E. Poem, Y. Berlatzky, J. Avron, D. Gershoni, B. D. Gerardot, and P. M. Petroff, Entangled Photon Pairs from Semiconductor Quantum Dots, Phys. Rev. Lett. **96**, 130501 (2006).

[17] R. M. Stevenson, R. J. Young, P. Atkinson, K. Cooper, D. A. Ritchie, and A. J. Shields, A semiconductor source of triggered entangled photon pairs, Nature (London) **439**, 179 (2006).

[18] R. Hafenbrak, S. M. Ulrich, P. Michler, L. Wang, A. Rastelli, and O. G. Schmidt, Triggered polarization-entangled photon pairs from a single quantum dot up to 30k, New J. Phys. **9**, 315 (2007).

[19] A. Dousse, J. Suffczynski, A. Beveratos, O. Krebs, A. Lemaître, I. Sagnes, J. Bloch, P. Voisin, and P. Senellart, Ultrabright source of entangled photon pairs, Nature (London) **466**, 217 (2010).

[20] E. del Valle, Distilling one, two and entangled pairs of photons from a quantum dot with cavity QED effects and spectral filtering, New J. Phys. **15**, 025019 (2013).

[21] M. Müller, S. Bounouar, K. D. Jöns, M. Glässl, and P. Michler, On-demand generation of indistinguishable polarization-entangled photon pairs, Nat. Photonics **8**, 224 (2014).

[22] A. Orieux, M. A. M. Versteegh, K. D. Jöns, and S. Ducci, Semiconductor devices for entangled photon pair generation: A review, Rep. Prog. Phys. **80**, 076001 (2017).

[23] T. Seidelmann, F. Ungar, A. M. Barth, A. Vagov, V. M. Axt, M. Cygorek, and T. Kuhn, Phonon-Induced Enhancement of Photon Entanglement in Quantum Dot-Cavity Systems, Phys. Rev. Lett. **123**, 137401 (2019).

[24] M. Cosacchi, J. Wiercinski, T. Seidelmann, M. Cygorek, A. Vagov, D. E. Reiter, and V. M. Axt, On-demand generation of higher-order Fock states in quantum-dot–cavity systems, Phys. Rev. Research **2**, 033489 (2020).

[25] J. Gea-Banacloche, Collapse and Revival of the State Vector in the Jaynes-Cummings Model: An Example of State Preparation by a Quantum Apparatus, Phys. Rev. Lett. **65**, 3385 (1990).

[26] M. Cosacchi, T. Seidelmann, J. Wiercinski, M. Cygorek, A. Vagov, D. E. Reiter, and V. M. Axt, Schrödinger cat states in quantum-dot-cavity systems, Phys. Rev. Research **3**, 023088 (2021).

[27] C. S. Muñoz, E. del Valle, A. G. Tudela, K. Müller, S. Lichtmannecker, M. Kaniber, C. Tejedor, J. J. Finley, and F. P. Laussy, Emitters of n-photon bundles, Nat. Photonics **8**, 550 (2014).

[28] Q. Bin, Y. Wu and X.-Y. Lü, Parity-Symmetry-Protected Multiphoton Bundle Emission, Phys. Rev. Lett. **127**, 073602 (2021).

[29] C. S. Muñoz, F. P. Laussy, E. del Valle, C. Tejedor, and A. González-Tudela, Filtering multiphoton emission from state-of-the-art cavity quantum electrodynamics, Optica **5**, 14 (2018).

[30] G. Diaz-Camacho, E. Zubizarreta Casalengua, J. C. López Carreño, S. Khalid, C. Tejedor, E. del Valle, and F. P. Laussy, Multiphoton emission, arXiv:2109.12049 [quant-ph].

[31] J. C. López Carreño, E. del Valle, and F. P. Laussy, Frequency-resolved monte carlo, Sci. Rep. **8**, 6975 (2018).

[32] M. Schmidt, M. von Helversen, M. López, F. Gericke, E. Schlottmann, T. Heindel, S. Kück, S. Reitzenstein, and J. Beyer, Photon-number-resolving transition-edge sensors for the metrology of quantum light sources, J. Low Temp. Phys. **193**, 1243 (2018).

[33] E. Schlottmann, M. von Helversen, H. A. Leymann, T. Lettau, F. Krüger, M. Schmidt, C. Schneider, M. Kamp, S. Höfling, J. Beyer, J. Wiersig, and S. Reitzenstein, Exploring the Photon-Number Distribution of Bimodal Microlasers with a Transition Edge Sensor, Phys. Rev. Applied **9**, 064030 (2018).

[34] M. Schmidt, I. H. Grothe, S. Neumeier, L. Bremer, M. von Helversen, W. Zent, B. Melcher, J. Beyer, C. Schneider, S. Höfling, J. Wiersig, and S. Reitzenstein, Bimodal behavior of microlasers investigated with a two-channel photon-number-resolving transition-edge sensor system, Phys. Rev. Research **3**, 013263 (2021).

[35] M. Bozzio, M. Vyvlecka, M. Cosacchi, C. Nawrath, T. Seidelmann, J. C. Loredo, S. L. Portalupi, V. M. Axt, P. Michler, and P. Walther, Enhancing quantum cryptography with quantum dot single-photon sources, npj Quantum Information **8**, 104 (2022).

[36] W. Denk, J. H. Strickler, and W. W. Webb, Two-photon laser scanning fluorescence microscopy, Science **248**, 73 (1990).

[37] N. G. Horton, K. Wang, D. Kobat, C. G. Clark, F. W. Wise, C. B. Schaffer, and C. Xu, In vivo three-photon microscopy of subcortical structures within an intact mouse brain, Nat. Photonics **7**, 205 (2013).

[38] C. J. Rowlands, D. Park, O. T. Bruns, K. D. Piatkevich, D. Fukumura, R. K. Jain, M. G. Bawendi, E. S. Boyden, and P. T. So, Wide-field three-photon excitation in biological samples, Light: Science & Applications **6**, e16255 (2017).

[39] D. G. Ouzounov, T. Wang, M. Wang, D. D. Feng, N. G. Horton, J. C. Cruz-Hernández, Y.-T. Cheng, J. Reimer, A. S. Tolias, N. Nishimura, and C. Xu, In vivo three-photon imaging of activity of GCaMP6-labeled neurons deep in intact mouse brain, Nat. Methods **14**, 388 (2017).

[40] A. Escobet-Montalbán, F. M. Gasparoli, J. Nylk, P. Liu, Z. Yang, and K. Dholakia, Three-photon light-sheet fluorescence microscopy, Opt. Lett. **43**, 5484 (2018).

[41] Q. Bin, X.-Y. Lü, F. P. Laussy, F. Nori, and Y. Wu, *n*-Phonon Bundle Emission Via the Stokes Process, Phys. Rev. Lett. **124**, 053601 (2020).

[42] T. Seidelmann, F. Ungar, M. Cygorek, A. Vagov, A. M. Barth, T. Kuhn, and V. M. Axt, From strong to weak temperature dependence of the two-photon entanglement resulting from the biexciton cascade inside a cavity, Phys. Rev. B **99**, 245301 (2019).

[43] D. E. Reiter, T. Kuhn, M. Glässl, and V. M. Axt, The role of phonons for exciton and biexciton generation in an optically driven quantum dot, J. Phys.: Condens. Matter **26**, 423203 (2014).

[44] D. E. Reiter, T. Kuhn, and V. M. Axt, Distinctive characteristics of carrier-phonon interactions in optically driven semiconductor quantum dots, Adv. Phys.: X **4**, 1655478 (2019).

[45] L. Besombes, K. Kheng, L. Marsal, and H. Mariette, Acoustic phonon broadening mechanism in single quantum dot emission, Phys. Rev. B **63**, 155307 (2001).

[46] P. Borri, W. Langbein, S. Schneider, U. Woggon, R. L. Sellin, D. Ouyang, and D. Bimberg, Ultralong Dephasing Time in InGaAs Quantum Dots, Phys. Rev. Lett. **87**, 157401 (2001).

[47] B. Krummheuer, V. M. Axt, and T. Kuhn, Theory of pure dephasing and the resulting absorption line shape in semiconductor quantum dots, Phys. Rev. B **65**, 195313 (2002).

[48] V. M. Axt, T. Kuhn, A. Vagov, and F. M. Peeters, Phonon-induced pure dephasing in exciton-biexciton quantum dot systems driven by ultrafast laser pulse sequences, Phys. Rev. B **72**, 125309 (2005).

[49] D. P. S. McCutcheon, Optical signatures of non-Markovian behavior in open quantum systems, Phys. Rev. A **93**, 022119 (2016).

[50] A. Krügel, V. M. Axt, T. Kuhn, P. Machnikowski, and A. Vagov, The role of acoustic phonons for rabi oscillations in semiconductor quantum dots, Appl. Phys. B **81**, 897 (2005).

[51] A. J. Ramsay, T. M. Godden, S. J. Boyle, E. M. Gauger, A. Nazir, B. W. Lovett, A. M. Fox, and M. S. Skolnick, Phonon-Induced Rabi-Frequency Renormalization of Optically Driven Single InGaAs/GaAs Quantum Dots, Phys. Rev. Lett. **105**, 177402 (2010).

[52] J. Förstner, C. Weber, J. Danckwerts, and A. Knorr, Phonon-Assisted Damping of Rabi Oscillations in Semiconductor Quantum Dots, Phys. Rev. Lett. **91**, 127401 (2003).

[53] P. Machnikowski and L. Jacak, Resonant nature of phonon-induced damping of Rabi oscillations in quantum dots, Phys. Rev. B **69**, 193302 (2004).

[54] A. J. Ramsay, A. V. Gopal, E. M. Gauger, A. Nazir, B. W. Lovett, A. M. Fox, and M. S. Skolnick, Damping of Exciton Rabi Rotations by Acoustic Phonons in Optically Excited InGaAs/GaAs Quantum Dots, Phys. Rev. Lett. **104**, 017402 (2010).

[55] N. Makri and D. E. Makarov, Tensor propagator for iterative quantum time evolution of reduced density matrices. I. Theory, J. Chem. Phys. **102**, 4600 (1995).

[56] N. Makri and D. E. Makarov, Tensor propagator for iterative quantum time evolution of reduced density matrices. II. Numerical methodology, J. Chem. Phys. **102**, 4611 (1995).

[57] A. Vagov, M. D. Croitoru, M. Glässl, V. M. Axt, and T. Kuhn, Real-time path integrals for quantum dots: Quantum dissipative dynamics with superohmic environment coupling, Phys. Rev. B **83**, 094303 (2011).

[58] A. M. Barth, A. Vagov, and V. M. Axt, Path-integral description of combined Hamiltonian and non-Hamiltonian dynamics in quantum dissipative systems, Phys. Rev. B **94**, 125439 (2016).

[59] M. Cygorek, A. M. Barth, F. Ungar, A. Vagov, and V. M. Axt, Nonlinear cavity feeding and unconventional photon statistics in solid-state cavity QED revealed by many-level real-time path-integral calculations, Phys. Rev. B **96**, 201201(R) (2017).

[60] D. Najer, I. Söllner, P. Sekatski, V. Dolique, M. C. Löbl, D. Riedel, R. Schott, S. Starosielec, S. R. Valentin, A. D. Wieck, N. Sangouard, A. Ludwig, and R. J. Warburton, A gated quantum dot strongly coupled to an optical microcavity, Nature (London) **575**, 622 (2019).

[61] C. Schneider, P. Gold, S. Reitzenstein, S. Höfling, and M. Kamp, Quantum dot micropillar cavities with quality factors exceeding 250, 000, Appl. Phys. B **122**, 19 (2016).

[62] B. Krummheuer, V. M. Axt, T. Kuhn, I. D'Amico, and F. Rossi, Pure dephasing and phonon dynamics in GaAs- and GaN-based quantum dot structures: Interplay between material parameters and geometry, Phys. Rev. B **71**, 235329 (2005).

[63] Y.-T. Chough, H.-J. Moon, H. Nha, and K. An, Single-atom laser based on multiphoton resonances at far-off resonance in the jaynes-cummings ladder, Phys. Rev. A **63**, 013804 (2000).

[64] A. Vagov, M. D. Croitoru, V. M. Axt, T. Kuhn, and F. M. Peeters, Nonmonotonic Field Dependence of Damping and Reappearance of Rabi Oscillations in Quantum Dots, Phys. Rev. Lett. **98**, 227403 (2007).

[65] M. Glässl, L. Sörgel, A. Vagov, M. D. Croitoru, T. Kuhn, and V. M. Axt, Interaction of a quantum-dot cavity system with acoustic phonons: Stronger light-matter coupling can reduce the visibility of strong coupling effects, Phys. Rev. B **86**, 035319 (2012).

[66] M. R. Klaßen and D. E. Reiter, Optical signals to monitor the dynamics of phonon-modified rabi oscillations in a quantum dot, Annalen der Physik **533**, 2100086 (2021).

[67] A. Nazir and D. P. S. McCutcheon, Modelling exciton-phonon

interactions in optically driven quantum dots, J. Phys.: Condens. Matter **28**, 103002 (2016).

[68] S.-L. Ma, X.-K. Li, Y.-L. Ren, J.-K. Xie, and F.-L. Li, Antibunched *n*-photon bundles emitted by a josephson photonic device, Phys. Rev. Research **3**, 043020 (2021).

[69] K. M. Birnbaum, A. Boca, R. Miller, A. D. Boozer, T. E. Northup, and H. J. Kimble, Photon blockade in an optical cavity with one trapped atom, Nature (London) **436**, 87 (2005).

[70] M. Cosacchi, T. Seidelmann, F. Ungar, M. Cygorek, A. Vagov, and V. M. Axt, Transiently changing shape of the photon number distribution in a quantum-dot–cavity system driven by chirped laser pulses, Phys. Rev. B **101**, 205304 (2020).